AD-783 242

DEVELOPMENT AND APPLICATION OF THE ELECTRON BEAM FLUORESCENCE TECHNIQUE FOR VISUALIZING HYPERSONIC HIGH TEMPERATURE AIRFLOWS

H. F. Lee, et al

Ohio State University

Prepared for:

Air Force Flight Dynamics Laboratory

March 1974

UNCLASSIFIED

SECURITY CLASSIFICATION OF THIS PAGE (When Data Entered)

REPORT DOCUMENTATION PAGE		READ INSTRUCTIONS BEFORE COMPLETING FORM
1. REPORT NUMBER	2. GOVT ACCESSION NO.	3. RECIPIENT'S CATALOG NUMBER AD-783 242
4. TITLE (and Subtitle) DEVELOPMENT AND APPLICATION OF THE ELECTRON BEAM FLUORESCENCE TECHNIQUE FOR VISUALIZING HYPERSONIC HIGH TEMPERATURE AIRFLOWS		5. TYPE OF REPORT & PERIOD COVERED Interim 1 Nov 71 - 15 Sep 73 6. PERFORMING ORG. REPORT NUMBER
7. AUTHOR(s) H. F. Lee S. L. Petrie		8. CONTRACT OR GRANT NUMBER(s)
9. PERFORMING ORGANIZATION NAME AND ADDRESS See Block 18		10. PROGRAM ELEMENT, PROJECT, TASK AREA & WORK UNIT NUMBERS Project 1426, Task 142601 Work Units 14260110 and 14260117
11. CONTROLLING OFFICE NAME AND ADDRESS Air Force Flight Dynamics Laboratory (FXN) United States Air Force Wright-Patterson Air Force Base, Ohio 45433		12. REPORT DATE March 1974 13. NUMBER OF PAGES 49
14. MONITORING AGENCY NAME & ADDRESS(if different from Controlling Office)		15. SECURITY CLASS. (of this report) UNCLASSIFIED 15a. DECLASSIFICATION/DOWNGRADING SCHEDULE

16. DISTRIBUTION STATEMENT (of this Report)

Approved for public release; distribution unlimited.

17. DISTRIBUTION STATEMENT (of the abstract entered in Block 20, if different from Report)

18. SUPPLEMENTARY NOTES

H. F. Lee
AF Flight Dynamics Laboratory (FXN)
Wright-Patterson AFB, Ohio 45433

S. L. Petrie
The Ohio State University Research Found.
1314 Kinnear Road
Columbus, Ohio 43212

19. KEY WORDS (Continue on reverse side if necessary and identify by block number)

Electron beam flow visualization; Electron beam generator system; Electron Beam fluorescence technique; Double-pass schlieren system; Pebble-bed heated wind tunnel; Electron beam instrumentation; Hypersonic high temperature airflow visualizations; Photographic method in flow visualization; Cross flow visualization; Gas mixing flow visualization

20. ABSTRACT (Continue on reverse side if neces[illegible] and identify by block number)

The electron beam fluorescence technique has been employed for visualizing hypersonic airflows. A high current electron beam generator was used to provide electron beams with currents up to 20 ma at voltages up to 40 kV. Applications of the technique at low densities illustrate that many details of the flow field can be obtained in density regions where conventional optical systems fail to yield useful results. The value and versatility of the method is demonstrated by results obtained with a sharp cone model and advanced ramjet aircraft configuration in a Mach 10 airflow. Techniques

DD FORM 1 JAN 73 1473 EDITION OF 1 NOV 65 IS OBSOLETE

UNCLASSIFIED

SECURITY CLASSIFICATION OF THIS PAGE (When Data Entered)

for obtaining quantitative density measurements with photographic and/or photomultiplier techniques are discussed.

FOREWORD

This technical report was prepared by H. F. Lee of the Air Force Flight Dynamics Laboratory, Wright-Patterson Air Force Base, Ohio and S. L. Petrie of the Aeronautical and Astronautical Research Laboratory of the Ohio State University Research Foundation. The research reported here is the result of technical developments in two programs under Task 142601, "Diagnostic, Instrumentation and Similitude Technology", of Project 1426. One was Work Unit 14260117, "Electron Beam Excitation Techniques for Measuring Flow Properties Around High Speed Vehicles", Contract F33615-72-C-1023 with the Ohio State University Research Foundation. The other was in-house development carried out under Work Unit 14260110, "Development of Flow Analysis Diagnostics to Establish Simulated Aerothermodynamic Test Environments for Advanced Military Vehicles". H. F. Lee of the Air Force Flight Dynamics Laboratory was project monitor for the contract as well as development engineer for the in-house efforts and facility tests.

There are a number of individuals who contributed, either directly or indirectly, to this research. The authors wish to acknowledge the efforts of the following Air Force personnel: R. F. Carpenter for performing a part of the tests; G. W. Williams for monitoring the electron beam generator system; R. L. Lickert for photography; D. L. Sine, E. A. Johnston, W. E. Bennett, D. W. Renick, E. M. Marshall, R. V. Corbin and C. D. Schroeder for tunnel operations; R. R. Smith and W. A. Rockwell for tunnel data; and T. F. Sabick for model inspection.

This report covers work conducted from 1 November 1971 to 15 September 1973

The manuscript was released by the authors on 9 October 1973 for publication as a technical report.

ABSTRACT

The electron beam fluorescence technique has been employed for visualizing hypersonic airflows. A high current electron beam generator was used to provide electron beams with currents up to 20 ma at voltages up to 40 kV. Applications of the technique at low densities illustrate that many details of the flow field can be obtained in density regions where conventional optical systems fail to yield useful results. The value and versatility of the method is demonstrated by results obtained with a sharp cone model and advanced ramjet aircraft configuration in a Mach 10 airflow. Techniques for obtaining quantitative density measurements with photographic and/or photomultiplier techniques are discussed.

TABLE OF CONTENTS

LIST OF TABLES

LIST OF ILLUSTRATIONS

LIST OF ILLUSTRATIONS - (Continued)

LIST OF SYMBOLS

c	Constant depending on geometrical factors
I	Intensity
I_o	Intensity without quenching
J	Beam current
$k = \frac{\lambda_s 2}{Q_s}$	
M	Mach number
N_2	Molecular nitrogen at ground state
N_2^+	Molecular nitrogen at ionized state
P_c	Exhaust plume chamber pressure
P_∞	Free stream pressure
P_o	Reservoir pressure
Q_{i_s}	Cross section for excitation of species i by secondary electrons
Q_{i_T}	Total ionization cross section for species i
Q_o	Cross section for excitation by primary electrons
Q_s	Cross section for excitation by secondary electrons
Q_T	Total ionization cross section for a pure gas
R_e	Reynolds number
T_o	Reservoir temperature
X_i	Number density fraction of species i
α	Angle of attack or pitch
ϕ	Roll angle or roll
λ_s	Related to the mean free path for secondary electrons
ρ	Gas density
ρ_i	Gas density of species i

LIST OF SYMBOLS - (Continued)

ρ'	Quenching density
ρ'_i	Quenching density of species i

I. INTRODUCTION

It is well-known that conventional optical methods of flow visualization fail under low density conditions typical of hypersonic wind tunnel facilities. In particular, interferometer and schlieren techniques frequently yield only the structure of very strong shock waves in such flow fields, and additional details concerning boundary layer and wake structures cannot be examined.

Because of the failure of these methods in many hypersonic test facilities, various low density flow visualization techniques have been developed and are summarized in Ref. 1. These include excitation of gas molecules by electron impact produced by high-voltage dc or ac glow discharges, x-ray and ultraviolet absorption techniques, and the electron optical schlieren method. These techniques may provide rough quantitative density distributions within the flow field and/or provide correct density measurement, but require elaborate and expensive set-ups. Frequently, they give flow images which are of poor contrast.

The electron beam fluorescence technique has received considerable attention for the measurement and visualization of low density flows where conventional optical techniques become insensitive. In this technique, a narrow beam of electrons is projected across the flow field and the interaction of the electrons with gas particles produces a column of radiation nearly coincident with the beam. In certain ranges of gas density, the intensity of the electron beam-induced fluorescence varies linearly with gas density. Hence, if a photograph of the flow is taken, both qualitative and quantitative measurements can be obtained. A calibration of the sensitivity of the film can be used with standard film data reduction techniques to yield actual density distributions.

The electron beam can be traversed mechanically through the flow field or it can be swept through a prescribed total angle electromagnetically. High beam voltages are normally used to reduce the elastic scattering of electrons so that a thin beam is produced. By proper adjustment of the sweeping voltages, either the entire flow field can be illuminated or an arbitrary "two-dimensional" slice out of the flow field can be examined. This latter feature makes the electron beam particularly attractive for the examination of flows about complex aerodynamic shapes.

When the electron beam is mechanically traversed through the flow field,[1] time-exposure photographs can be obtained to yield visualization in arbitrary gas mixtures. In this case, however, the wind tunnel run time is long and only steady-state flow phenomena can be investigated.

Application of afterglow techniques requires the presence of long-lived excited particles in the flow field downstream of the electron beam; the afterglow method has been particularly successful in nitrogen[3,4] and helium[4,5] flow fields. However, attempts to employ either the

afterglow radiation or electromagnetic sweeping of the beam in hypersonic airflows has generally been unsuccessful. It is notable that visualization in airflows depends upon excitation of molecular nitrogen by high-speed electrons and it is well-known that nitrogen-oxygen collisions result in earlier quenching of radiation as the density is increased than do either in nitrogen-nitrogen, or in nitrogen-helium collisions.[7] In addition, no afterglow radiation outside the main area of excitation is observed in airflows while such observations are common in nitrogen and helium. The afterglow radiation is responsible, in part, for the successful application of a swept electron beam in nitrogen and helium. Radiation from the gas is observed even after the electron beam has passed so that sufficient radiation intensities are present for the application of conventional photographic techniques. The absence of the afterglow radiation in airflows may be responsible for past failures of the method.

In usual applications of the electron beam for flow visualization, electron beams with voltages from 10 to 100 kV and beam currents of a few milliamperes are employed. It is expected that application of image intensifier techniques[7] to airflows will yield useful visualization data. However, this requires complicated photographic equipment. Another approach to obtain useful data is to employ an electron beam with a current high enough to yield sufficient photographic exposure in the absence of afterglow radiation. The results of such an application are reported here.

A high current electron beam was used to provide visualization of low density airflows. Particular emphasis was placed on flow regimes where conventional schlieren techniques yield little or no useful data. Combined schlieren and electron beam data were obtained at certain wind tunnel operating conditions to allow comparisons of the sensitivities of the two systems.

Partial results were published in Refs. 8 and 9. This technical report summarizes the effort devoted to development and application of the electron beam fluorescence technique for visualizing hypersonic, high temperature airflows.

The complete visualization system is described in Section II and particular emphasis is placed on the high current electron beam generator. Typical results from application of the technique to complicated aerodynamic flow fields are presented in Section III. Important factors to be considered for quantitative density determinations are examined in Section IV. Finally, the conclusions are given in Section V.

II. APPARATUS AND PROCEDURES

A. WIND TUNNEL AND MODEL SYSTEMS

The flow visualization studies were conducted in the High Temperature Facility (HTF) operated by the Flight Mechanics Division of the Air Force Flight Dynamics Laboratory (AFFDL). The facility consists of a pebble-bed heater, a contoured convergent-divergent nozzle, a free-jet test cabin, and a pressure recovery system. For the studies reported here, the tunnel was operated with air at a reservoir temperature of 2500°R with reservoir pressures varying from 100 to 600 psia. The nominal nozzle exit Mach number was 10.

To establish the feasibility of obtaining quantitative data from the flow visualization technique, a series of wind tunnel tests was conducted with a sharp 9° half-angle cone at various angles of attack. The cone was fitted with an annular injection port at its base so that massive base blowing could be simulated. Both air and helium were used for the plume gas.

Visualization of the flow about an advanced ramjet aircraft configuration was obtained to illustrate application of the technique to complicated aerodynamic shapes. This model was mounted on a pitch-roll mechanism such that arbitrary combinations of angles of attack and roll could be obtained. The model and the sting-type roll mechanism are shown in Figures 1 and 2.

A Sheffield Cordax measuring machine was utilized for measurements of the coordinates of the ramjet fighter model. The data were recorded on paper tape and a digital computer was used to transform the coordinate information into graphical form.[10] Typical results of cross sections in the transverse direction are presented in Figures 3 and 4. In Figure 4, the solid line represents a profile of the right hand side of the model looking from the tail toward the nose of the model. The plus signs represent the locations of points on the left hand side reflected to the right hand side. All of the measurements are obtained in the same vertical plane. Similar plots can be generated in the longitudinal direction.

B. ELECTRON BEAM SYSTEM

The electron beam generator is shown schematically in Figure 5 and is described in detail in Ref. 11. It consists of a duoplasmatron electron source, electrostatic lenses for beam forming, and electromagnetic beam steering and focusing systems. An einzel lens is used for beam voltages up to 20 kV; a gap lens is used for voltages above 20 kV. The lens elements are mounted inside a 6-inch standard steel tee which is connected to a 6-inch oil diffusion pump. A baffle is used between the diffusion pump and the beam chamber to reduce

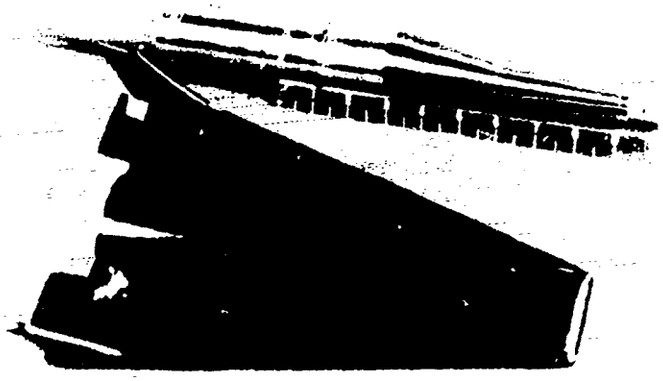

Figure 1. Roll Mechanism and Top View of Ramjet Fighter Model

Figure 2. Roll Mechanism and Side View of Ramjet Fighter Model

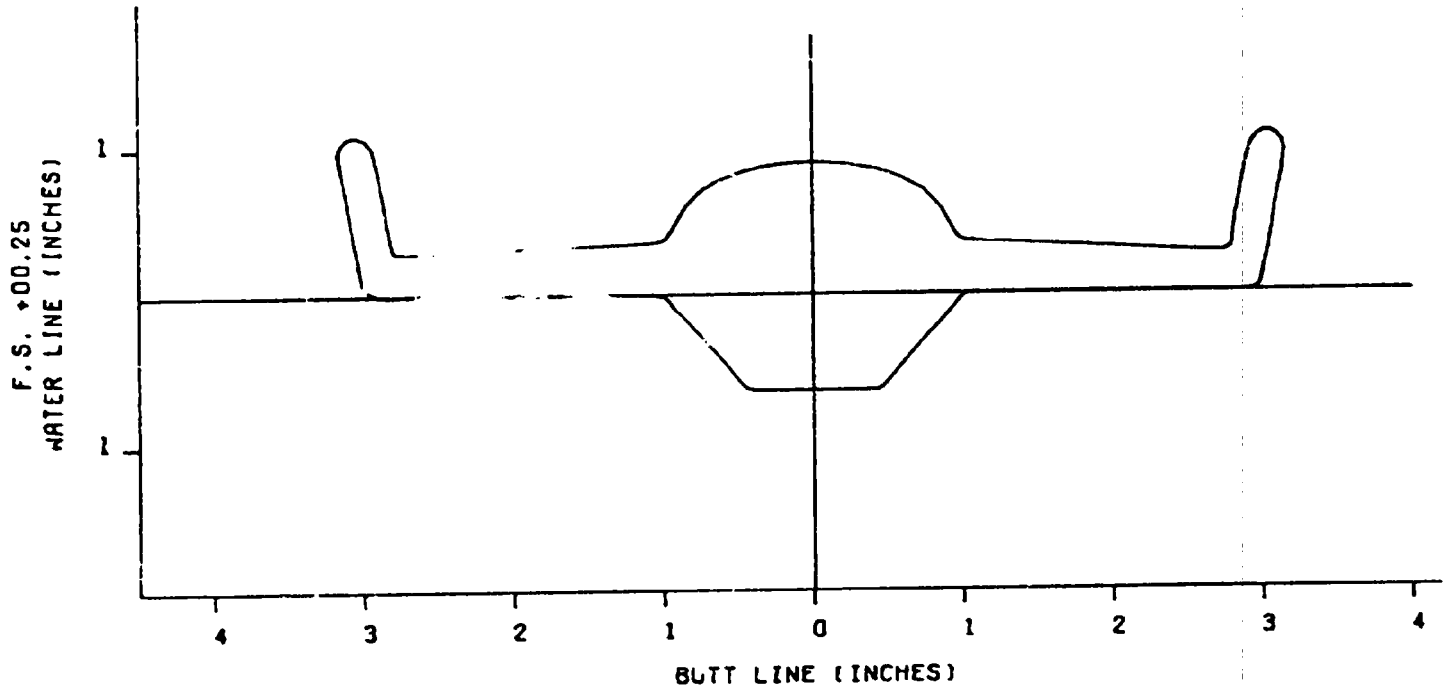

Figure 3. Cross Section : Ramjet Fighter at Fuselage Station 0.25"

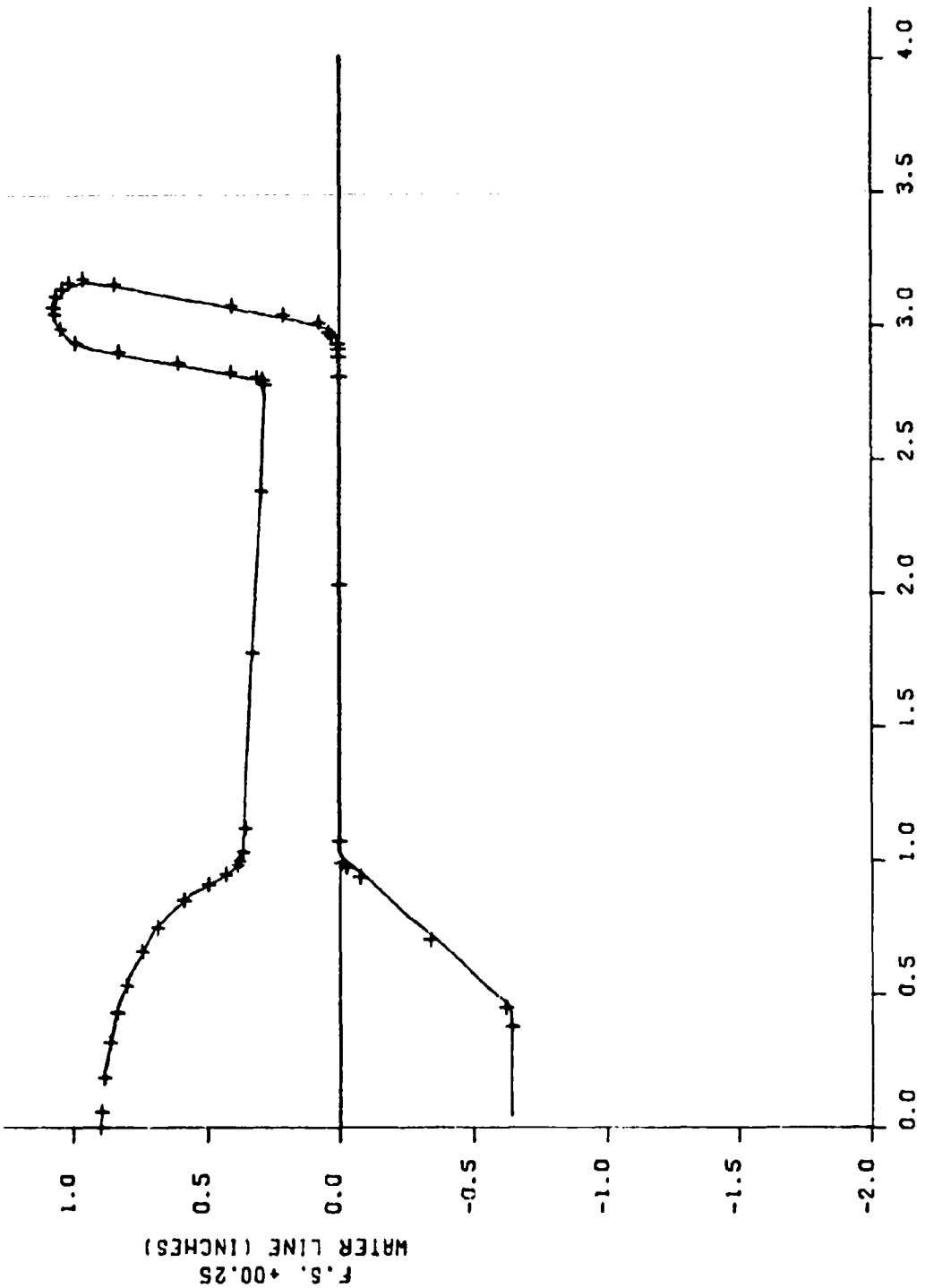

Figure 4. Sectional Symmetry Plot of Ramjet Fighter at Fuselage Station 0.25"

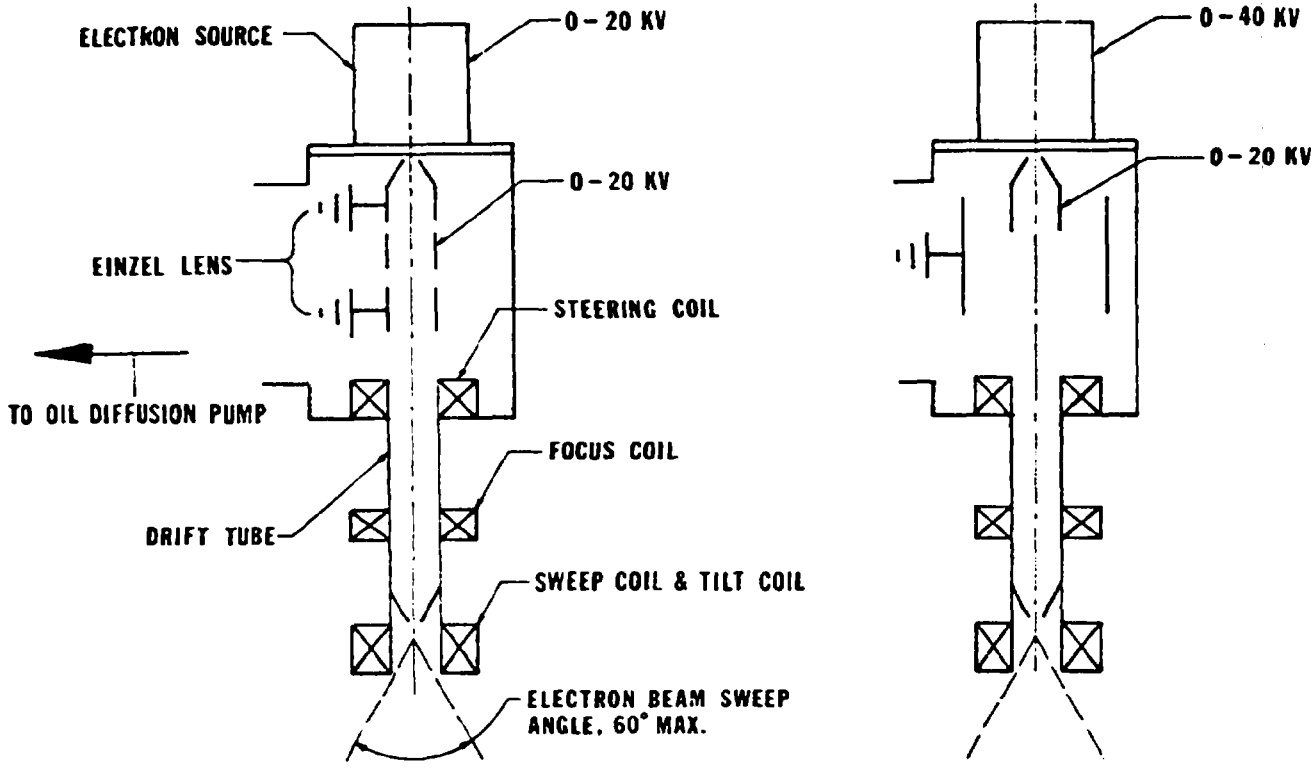

a) Einzel Lens for Operation up to 20 kV b) Gap Lens for Operation up to 40 kV

Figure 5. Electron Beam Generator Schematics

backstreaming of the diffusion pump oil. The electrons exit from the beam chamber through a 0.03-inch diameter exit orifice to the bell-shaped exit. The entire assembly is mounted inside the wind tunnel test cabin such that the electron beam is projected downward through the nozzle centerline. The electron beam power supplies and vacuum control console are located in a control panel adjacent to the tunnel. The beam generator is electrically isolated from the test cabin so that no special beam collecting devices are required; that is, the tunnel test cabin serves as a beam receiver.

The maximum acceleration potential is 75,000 V with a maximum beam current of 60 ma. To minimize defocusing of the beam as it traverses the drift tube and passes through the exit orifice, the electrons are accelerated from high potentials toward ground potential. Hence, the electron beam power supplies must be operated at high potential, and electrical isolation from ground must be maintained.

Electromagnetic sweeping of the beam is accomplished with a sweep coil located immediately beneath the exit orifice. A triangular current wave form in the deflection coil generally is best suited for flow visualization work, since the electron beam moves at a constant rate and will yield a constant exposure with deflection angle on the film. In addition, a high sweep frequency is desirable to provide many passes of the electron beam during the photographic exposure time. (For example, a 60 Hz sweep frequency will yield some "flicker" in movies taken at 24 frames per second.)

In addition to sweeping the beam, the tilt coil can be used to locate the electron beam in any desired position within the test gas. A dc bias system is supplied to provide an offset current through both sets of coils making up the deflection yoke. The sweeping voltage is capacitance-coupled to one set of coils. Adjustment of the plane of the sweep is accomplished simply by rotating the deflection yoke on the drift tube.

The electron beam generator installation in the HTF is shown schematically in Figure 6. The test configuration with the ramjet fighter aircraft model is shown in Figure 7. The bell-shaped exit of the sweep coil is visible at the upper left of this photograph. The high voltage cable to the electron source and the duoplasmatron enclosure are pressurized with sulfur hexafluoride (SF_6) to prevent arcing. Electric wires to the oil diffusion pump heater and to the cold cathode pressure gage are vented to the atmosphere to eliminate electric breakdown caused by low pressures in the test cabin.

A Victoreen Model 440 RF radiation exposure rate measuring system was utilized to monitor the radiation levels in the vicinity of the wind tunnel test cabin. This detector was calibrated by the Health Physics Group at Wright-Patterson Air Force Base. The radiation levels under all test conditions were so low (< 0.25 mR/hr) that no special precautions were needed. As expected, it was noted that the intensity of the soft

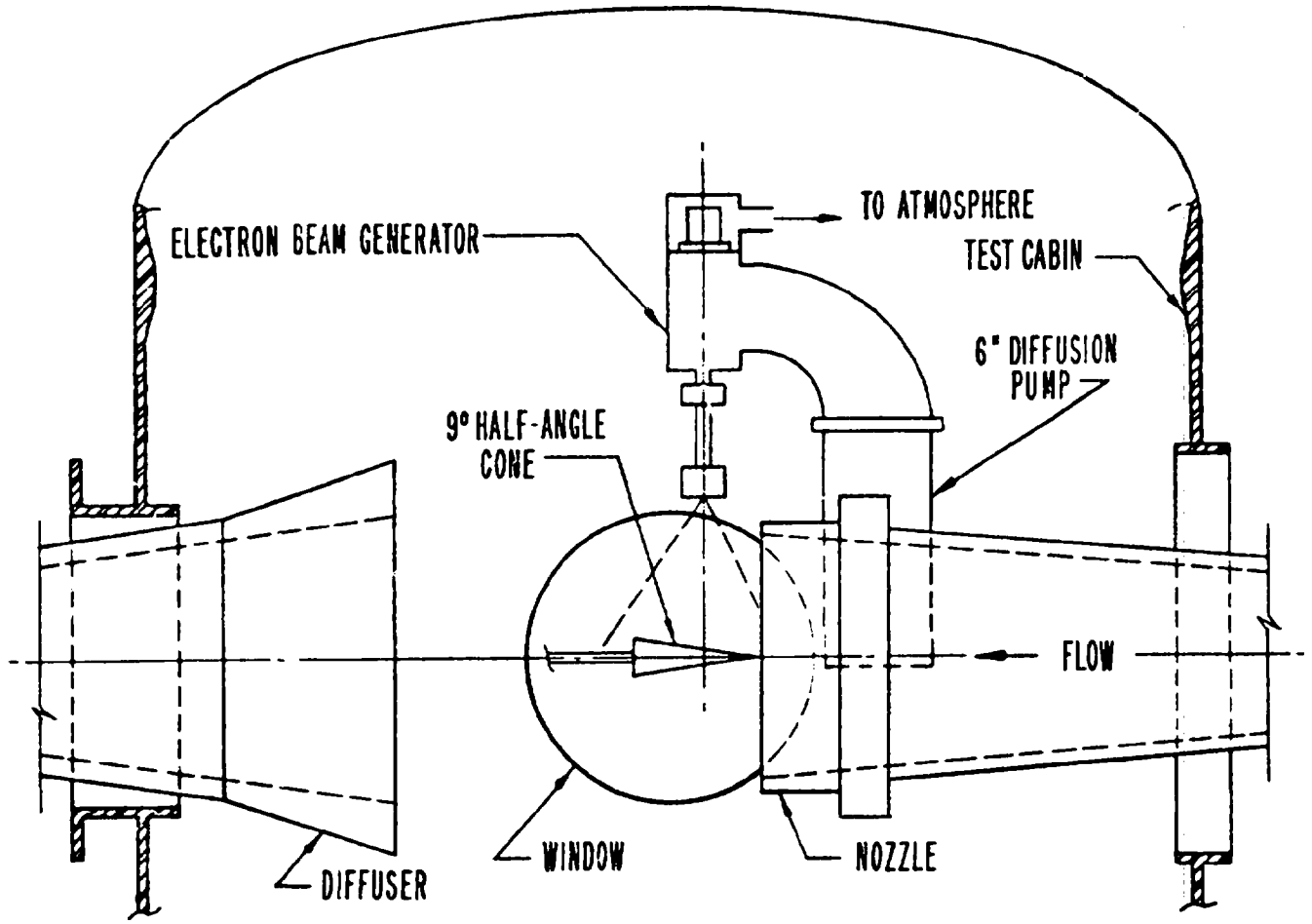

Figure 6. Electron Beam Installation in AFFDL/HTF

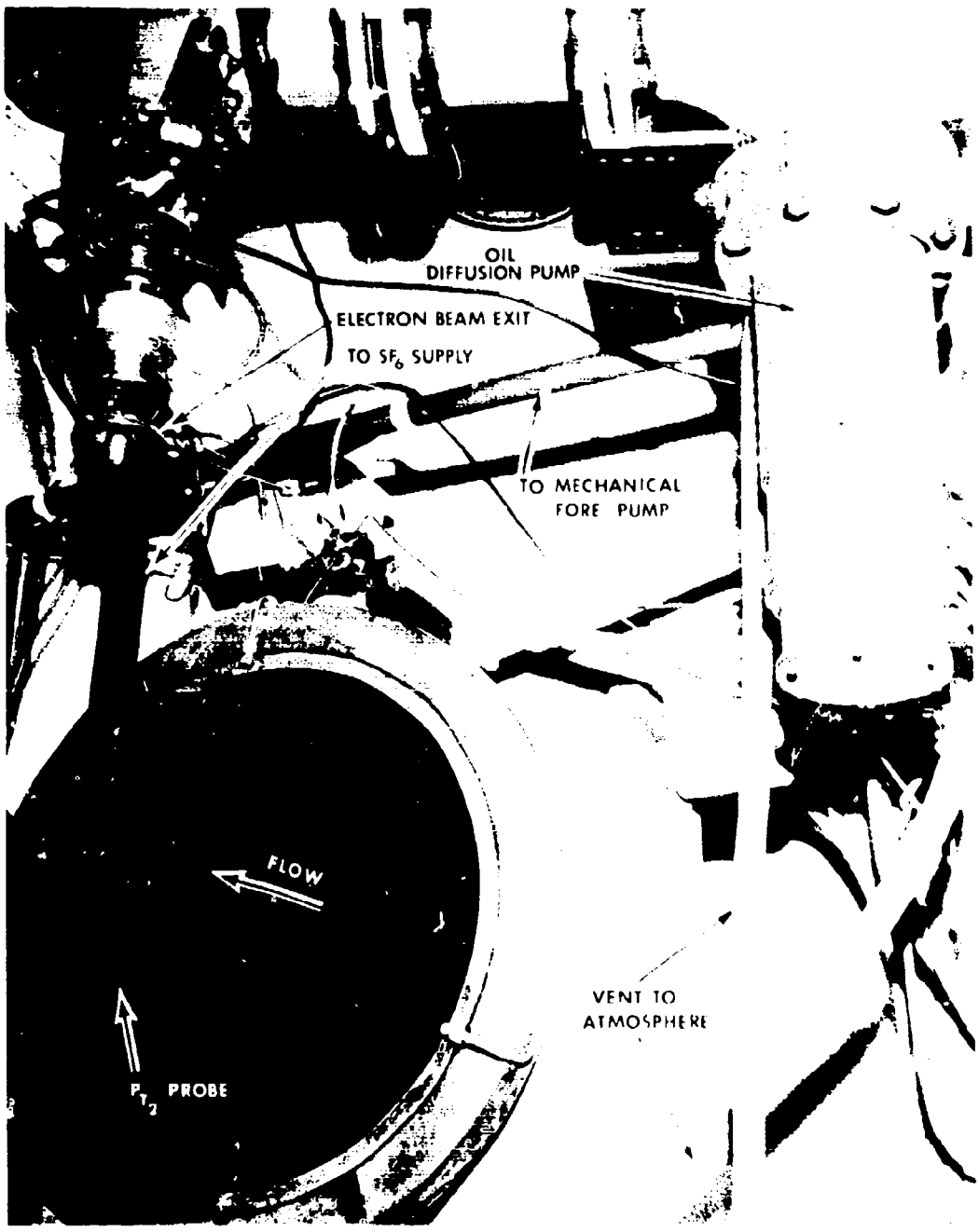
OIL
DIFFUSION PUMP
ELECTRON BEAM EXIT
TO SF_6 SUPPLY
TO MECHANICAL
FORE PUMP
FLOW
VENT TO
ATMOSPHERE
P_{T_2} PROBE

x-rays decreased as the model material was changed from copper to steel and from steel to aluminum.

C. DOUBLE-PASS SCHLIEREN SYSTEM

The double-pass schlieren system consists of a parabolic mirror, a plane mirror (each has an adjustable stand) and the remaining optics mounted on an optical bench. All optics on the bench are located on the centerline of the parabolic mirror. The test region and the plane mirror are in the upper half of the parallel beam from the large parabolic mirror.

The light source is an Osram HBO 200 W short-arc mercury lamp. The light from the lamp is focused on a 1/2 mm square aperture which serves as the entrance slit for the schlieren system. This slit is located at the focus of the parabolic mirror. The parallel light reflected from the parabolic mirror passes through the test cabin and is reflected back through the cabin again, to the parabolic mirror through a beam splitter and a magnifying lens to a horizontal knife edge, another beam splitter, and a camera lens to a 35 mm camera body as shown in Figure 8.

III. EXPERIMENTAL RESULTS

A. PHOTOGRAPHIC METHOD

To establish the required exposure times for the various photographic equipment employed during the wind tunnel tests, a series of static experiments was conducted. The HTF test cabin was evacuated to maintain the static pressure over a range from 1 Torr up to 5 Torr, and the electron beam was swept at 60 Hz to determine the appropriate exposure times of Polaroid B&W Type 52 (ASA 400) and Polaroid Polarcolor Type 58 (ASA 75) films. These pressure conditions bracketed the expected gas densities in the flow fields about the body. After a series of static calibrations, the feasibility of obtaining flow patterns by the photographic method was firmly established.

The electron-induced radiation was photographed with a variety of films using 4 in. by 5 in. and 35 mm cameras, as well as 16 and 35 mm movie cameras. Details of the films, the model and the tunnel operating conditions are summarized in Tables I and II. Photographs also were obtained with the double-pass schlieren system under the same test conditions as those employed with the electron beam.

During the static calibrations, a thermocouple was soldered on the surface of a steel cone model at the centerline of sweeping electron beam. The temperature rise for a 3-minute duration (nominal tunnel run time) amounted to less than 10°F for static pressures from 1 to 5 Torr.

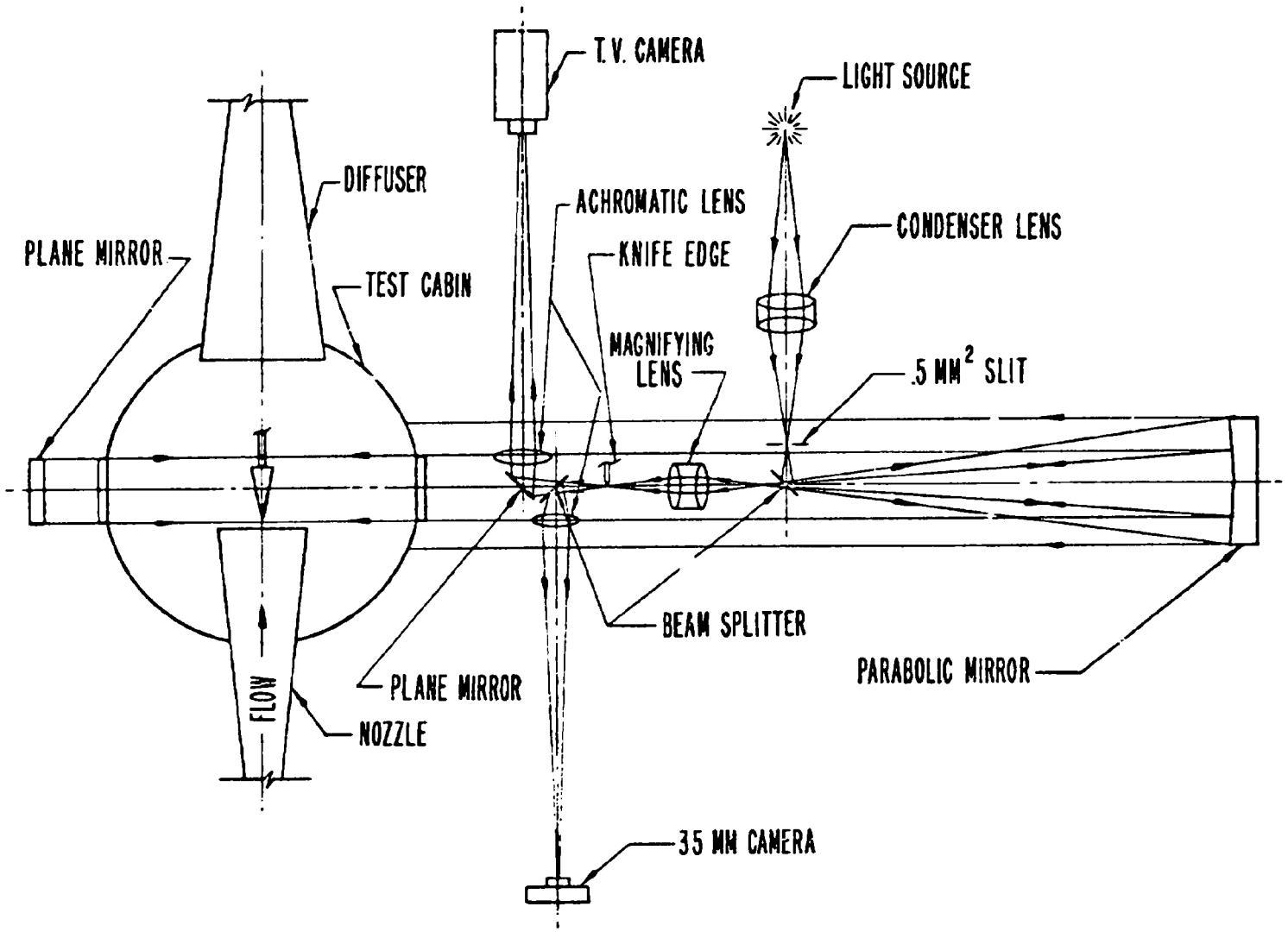

Figure 8. AFFDL/HTF 20-Inch Diameter Double-Pass Schlieren System

TABLE I. SUMMARY OF FILM DATA FOR SCHLIEREN AND ELECTRON BEAM PHOTOGRAPHS IN PARALLEL FLOW

Fig. No.	Film Type	ASA	Speed	f/no.	P_o(psia)	Remarks
9	Ektachrome 35 mm	320	16 fps	2.3	300	Electron Beam Movies
10	Ektachrome 35 mm	320	16 fps	2.3	300	Electron Beam Movies
11	Ektachrome 35 mm	320	16 fps	2.3	200	Electron Beam Movies
13	Polaroid 52	400	1/2 sec	6.3	300	Air Blowing
14	Ektachrome 35 mm	320	16 fps	2.3	300	Air Blowing
15a	GAF 35 mm	500	1/500 sec	19	600	Schlieren
16a	GAF 35 mm	500	1/500 sec	19	600	Schlieren
17a	GAF 35 mm	500	1/500 sec	19	600	Schlieren
18a	Ektachrome 35 mm	320	16 fps	2.3	600	Electron Beam Movies
19a	Ektachrome 35 mm	320	4 fps	3.5	200	Sequence Camera
15b	Kodak Double-X 35 mm	250	24 fps	2.2	600	Electron Beam Movies
16b	Kodak Double-X 35 mm	250	24 fps	2.2	600	Electron Beam Movies
17b	Kodak Double-X 35 mm	250	24 fps	2.2	600	Electron Beam Movies
18b	Ektachrome 35 mm	320	16 fps	2.3	600	Electron Beam Movies
19b	Ektachrome 35 mm	320	4 fps	3.5	600	Sequence Camera

TABLE II. FILM DATA FOR ELECTRON BEAM PHOTOGRAPH IN CROSS FLOW

Fig. No.	Film Type	ASA	Speed	f/no.	P_o(psia)	Remarks
21	Polaroid 52	400	1/4 sec	6.3	300	Cone

Since the reservoir temperature was 2500°R for all test runs, it was safe to assume that the temperature increase due to impingement of the electron beam on the model was negligible.

B. INFLUENCES OF ANODIZED MODEL SURFACES

The effect of model surface reflection was briefly investigated. The purpose of anodizing model surfaces is to minimize surface reflections, and comparative results are shown in Figures 9 and 10. Figure 9 was obtained with an anodized model while the model of Figure 10 was unanodized. Because of reflection from the model surface, Figure 10 gives the impression that the far side tail fin is located within the bow shock. However, as can be seen in Figure 9, the tail fin is actually outside the region of excitation by the electron beam. Bright reflections along the model body also are evident in Figure 10. Thus, the anodized model was adopted for flow visualization tests to avoid any misinterpretation of photographic or visual results.

When the ramjet fighter is rotated such that both the model body and one of its tail fins are in the direct path of the electron beam, the bow shock and tail fin shock can be readily visualized, as shown in Figure 11.

The sting-type roll mechanism as shown in Figures 1 and 2 was attached inside the body of the test model through a set screw. The temperature of the model and the roll mechanism increases after successive tunnel runs. Consequently, as shown in Figure 12, both the model and the sting were cooled with compressed CO_2 at the conclusion of a tunnel run.

C. COMPARISONS OF ELECTRON BEAM AND SCHLIEREN FLOW VISUALIZATION

1. Cone Flow

Electron beam and schlieren photographs of the cone flow field were obtained with various amounts of base-blowing. At the 100 psia operating condition, schlieren failed to show the bow shock wave while the electron beam yielded visualization of the entire flow field. At the 300 psia pressure, only the bow shock was observable in the schlieren photographs, while the electron beam gave shock layer and wake details. When helium was used for the base blowing, color photography could be used to examine the extent of helium diffusion throughout the flow field. The electron-induced radiation in helium is most intense in the region near 5900 Å; while that in air is most intense near 4000 Å.

In Figure 13 the separation on the cone surface caused by the interaction of the plume with the cone shock layer is clearly observable. Figure 14 shows a shock wave present in the cone wake. The wave is

Figure 9. Electron Beam View of Anodized Ramjet Fighter at 10° Roll and 0° Pitch

Figure 10. Electron Beam View of Unanodized Ramjet Fighter at 10° Roll and 0° Pitch

Figure 11. Electron Beam Photograph of Ramjet Fighter at 10° Roll and 0° Pitch

Figure 12. Cooling Roll Mechanism and Test Model with CO_2 after Tunnel Run

Figure 13. Electron Beam View of Exhaust Plume Interaction with Conical Flow Field

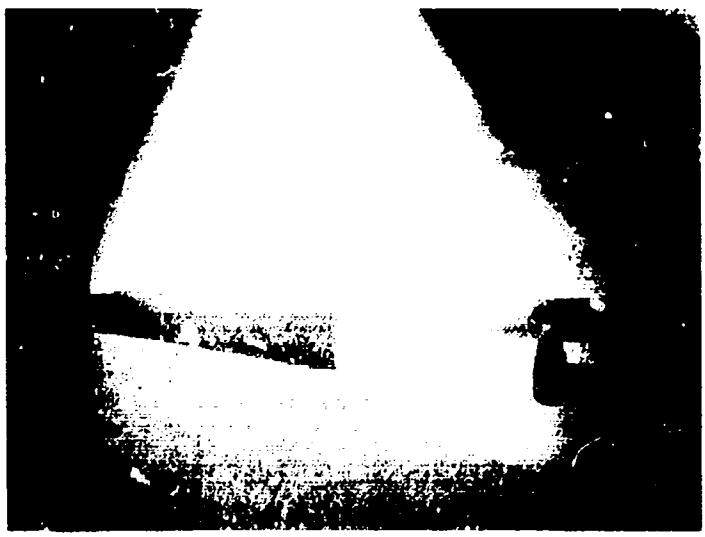

Figure 14. Electron Beam View Showing Wave in Cone Flow Wake

caused by downstream pressure influences and its unsteady behavior was studied with 35 mm movies. The photograph of Figure 14 is a reproduction of one frame of these movies.

Another feature of the electron beam diagnostic technique is evident in Figures 13 and 14. The presence of the model with base blowing causes sufficient blockage of the tunnel to raise the test cabin pressure, which forces an oblique shock to form at the nozzle exit. In low Reynolds number studies when the quality of the flow is questioned, it must be examined with pitot probes, since conventional schlieren systems show few flow details at these densities. Probing of the flow with a pitot probe is a perturbing and time consuming process as well as having a limited response to dynamic effects. However, the formation of the nozzle exit shock wave can clearly be seen in the electron beam photographs of Figures 13 and 14. The nozzle exit shock wave also can easily be observed with the naked eye at the test scene.

The beam was operated in the sweeping mode for all of the electron beam photographs. Preliminary experiments were conducted to determine if there was any afterglow radiation sufficient for photographic purposes. No afterglow was observed and the radiation was restricted to the region excited by the primary electrons.

2. Ramjet Fighter

An extensive series of photographs was taken of the flow field about the ramjet fighter aircraft configuration. The pitch-roll mechanism was either set at a fixed angle of attack while the model was rolled at a constant speed of 1 rpm, or the model was held at a fixed roll angle and was pitched at an average speed of 12°/sec. Two 35 mm cameras were employed for both the schlieren and electron beam photographs. The camera used for the electron beam photographs viewed the model from the side of the test cabin opposite the schlieren camera and was positioned at an angle of 69° above the horizontal plane passing through the tunnel centerline. The schlieren system was placed in the horizontal plane. Reproduction of comparative frames from the schlieren camera and the electron beam movies are shown in Figures 15-17.

Figures 15-17 were obtained at the 600 psia operating condition. Figures 15 and 16 illustrate the "sectional view" capability of electron beam visualization; while schlieren integrates all effects along its field of view, selective sectional regions in the plane of sweep can be examined with the electron beam.

The relative sensitivities of the schlieren and electron beam systems are well illustrated by Figure 17. In this case, with the model rolled such that the upper surface is observed, the integrating effects of the schlieren system are minimized. The shock structure does not appear in the schlieren photograph but is clearly visible with the electron beam system.

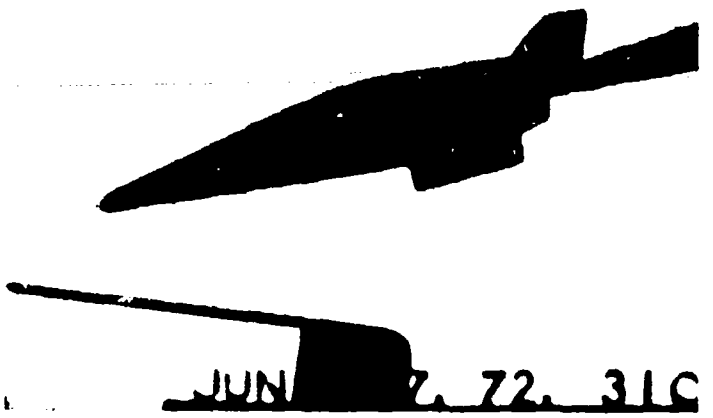

(a) Schlieren Photograph

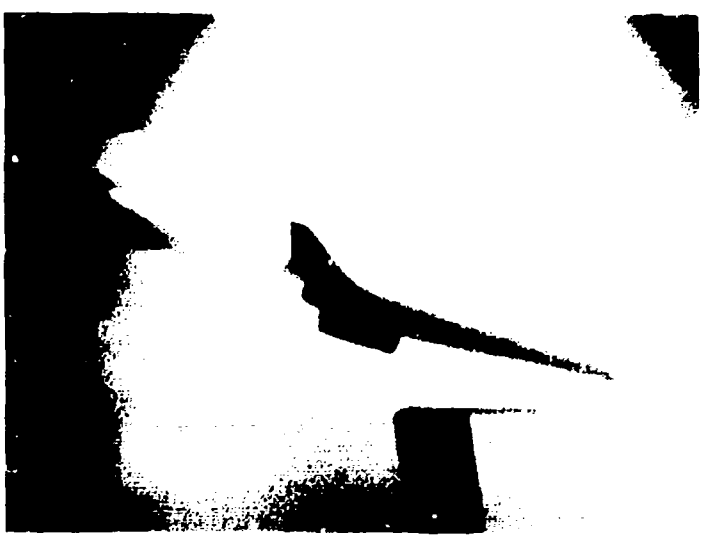

(b) Electron Beam Photograph

Figure 15. Ramjet Fighter at 0° Roll and -15° Pitch

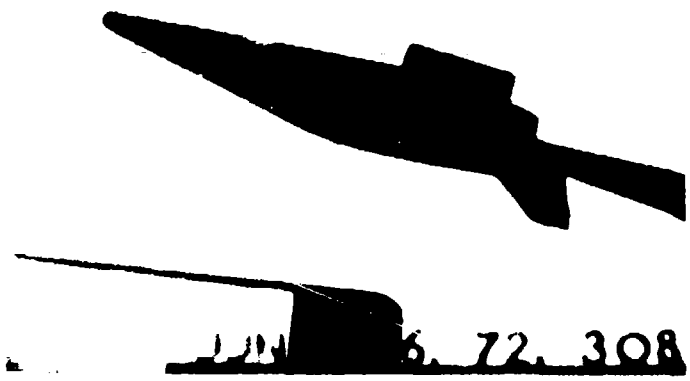

(a) Schlieren Photograph

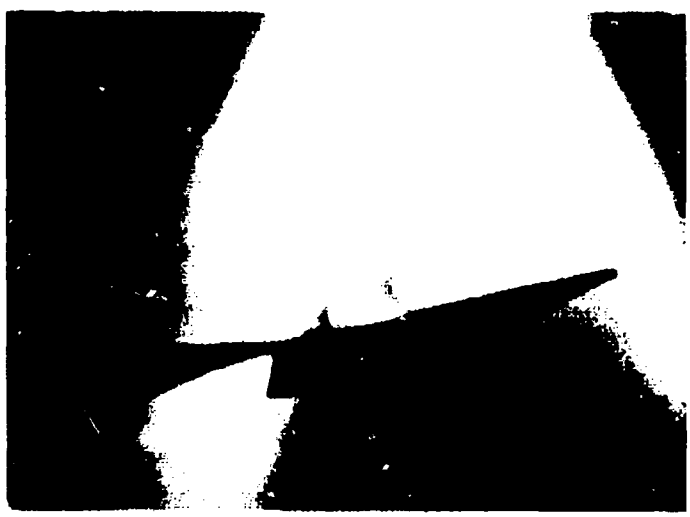

(b) Electron Beam Photograph

Figure 16. Ram, et Fighter at 180° Roll and 15° Pitch

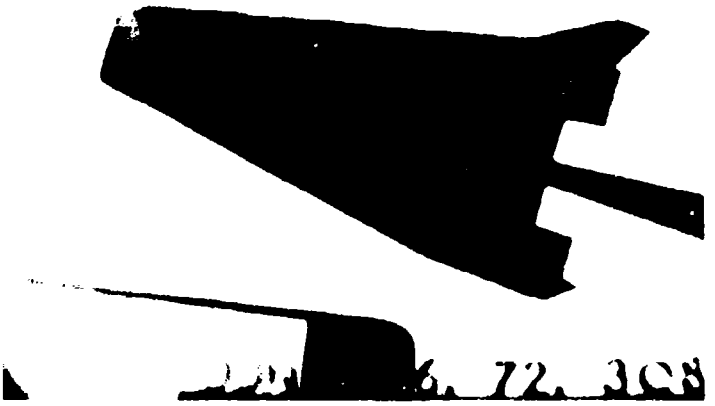

(a) Schlieren Photograph

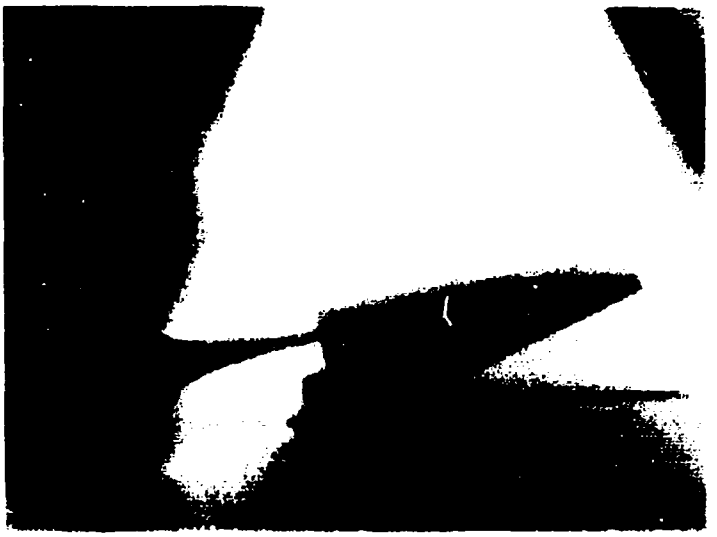

(b) Electron Beam Photograph

Figure 17. Ramjet Fighter at 270° Roll and 15° Pitch

The photographs shown in Figures 18a and 18b were taken at the 600 psia operating point with the model at 25° pitch, 0° and 180° roll, respectively. The bow shock generated by the ramjet fighter and the oblique shock formed at the nozzle exit due to the tunnel blockage caused by the large angle of attack are easily identifiable. These photographs are reproductions of two frames of 35 mm movies. The exact angle of attack at which the nozzle-exit shock wave begins to occur and the angle of attack at which the tunnel flow "break down" can be obtained from the 35 mm movies by examining appropriate frames. These model angles of attack were found to be 22.5° and 30°, respectively.

The main disadvantage of the electron beam method is that only half of the model flow field can be viewed at any one time. Hence, two photographs and a combined pitch and roll of the model are required to show both the expansion and compression sides of the model. The color photographs shown in Figure 19 illustrate this point vividly. This disadvantage of the electron beam method could be eliminated with a dual electron beam system, but such complexity is warranted only in very special applications.

As can be seen in Figure 19, the boundary layer along the model surface on the expansion side (Fig. 19a) is much thicker than on the compression side (Fig. 19b). On the expansion side, the separation of the bow shock wave and boundary layer is evident; while on the compression side, the bow shock, the cowling shock and the boundary layer are nearly superimposed.

Figure 19 was taken with a 35 mm sequence camera located on the horizontal plane passing through the tunnel centerline and at an angle of 60° measured from the upstream direction toward the center of the test cabin. Therefore, a small part of the model leading edge was hidden by the nozzle exit. Film data are included in Table I.

The electron beam photographs in this report were reproduced by one of the following four step sequences:

(1) Ektachrome 35 mm positive film (a selected frame from movies), reproduced to Kodacolor 4" x 5" negative film, copied to color contact print and then to a color reproduction (print in this report).

(2) Ektachrome 35 mm positive film (a selected frame from movies), reproduced to Royal-X Pan 4" x 5" negative film, copied to B&W contact print and then to a B&W reproduction (print in this report).

(3) Double-X 35 mm positive film (a selected frame from movies), reproduced to Royal-X Pan 4" x 5" negative film, copied to B&W contact print and then to a B&W reproduction (print in this report).

(a) At 0° Roll and 25° Pitch

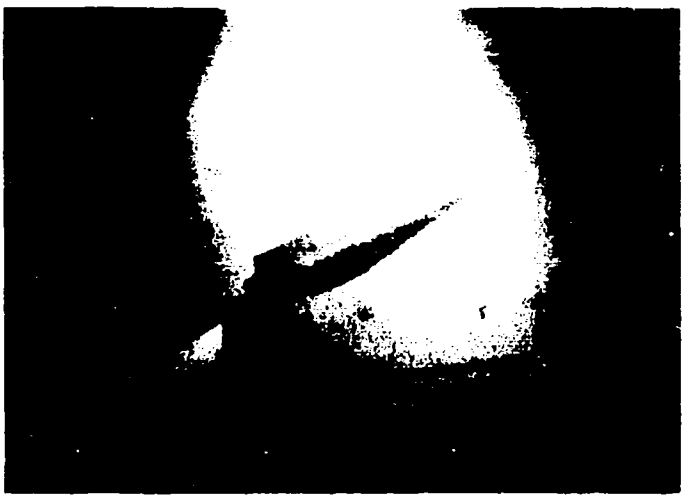

(b) At 180° Roll and 25° Pitch

Figure 18. Electron Beam Photographs of Ramjet Fighter Indicating Bow Shock, Oblique Shock and Boundary Layer

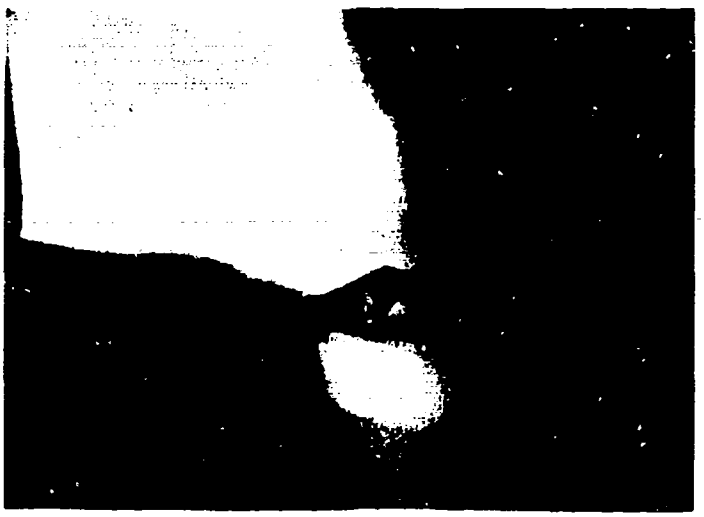

(a) Expansion Side: 0° Roll and 15° Pitch

(b) Compression Side: 180° Roll and -15° Pitch

Figure 17. Electron Beam Views Exhibiting Expansion and Compression Sides of Research Fighter in Color

(4) Polaroid 52 4" x 5" positive print, reproduced by Royal-X Pan 4" x 5" negative film (for permanent record), copied to B&W contact print and then to a B&W reproduction (print in this report).

As a rule, the image quality degrades as a result of each reproduction step.

The color tone-reproduction is not very well preserved under the complexity of the multiple step reproduction techniques. Even a direct color Polaroid photograph improves the fidelity only slightly. In fact, the electron beam fluorescent scene which appears predominantly violet in human vision becomes blue in the color photographs. Color photographs are easier to interpret than the black and white reproductions, as shown in Figure 20.

3. Cross Flow Visualization

All the electron beam photographs of the previous figures depict sectional slices of flow patterns in the direction parallel to the flow direction with the electron beam generator operating at a voltage of 20 kV and a current of 20 ma. The electron beam generator operating at these conditions produces an apparent depth of field of approximately 3" at the tunnel centerline (which is approximately 22" below the exit orifice of electron beam).

To obtain a sharp definition in the plane normal to the flow direction (henceforth abridged as the cross flow direction), the electron beam generator must be operated at a voltage near 40 kV. This reduces the elastic scattering of electrons and increases the spatial resolution, which reduces the apparent depth of field from about 3" to 1". Figure 21 shows the cross section of a conical shock wave generated by the cone model in the cross flow direction. A similar photograph cannot be obtained with a schlieren system. The film data for this electron beam view is given in Table II.

D. EDITING MOVIES

One 16 mm movie camera was used to establish the correct exposures. These exposures depend on parameters such as the number of frames per second (fps), type of film, f/no., model shape, tunnel and electron beam operating conditions and rate of model movement in pitch and/or roll. Three separate cameras were used during a tunnel run. Two 35 mm movie cameras, one with color film was positioned at 69° above the horizontal plane passing through the tunnel centerline, and the other with black and white film was located symmetrically on the opposite side. The third camera was a 35 mm sequence camera loaded with color film and positioned on the horizontal plane passing through the tunnel centerline and at an angle of 60° measured from the upstream direction toward the center of the test cabin. All movies were taken with positive films for easy reviewing of the results.

(a) Expansion Side: 0° Roll and 15° Pitch

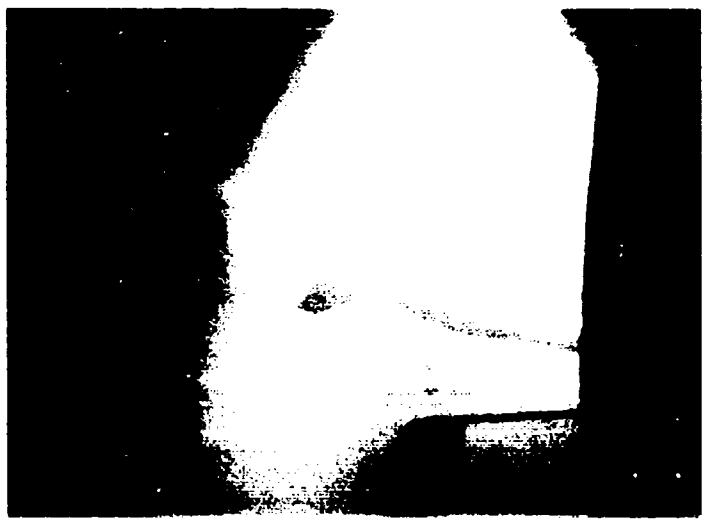

(b) Compression Side: 180° Roll and -15° Pitch

Figure 20. Electron Beam Views Exhibiting Expansion and Compression Sides of Fanjet Fighter in Black and White

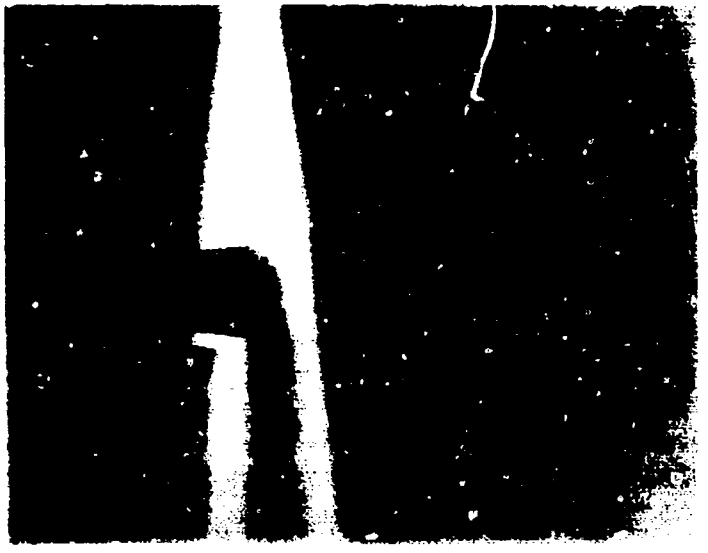

Figure 21. Electron Beam View Showing Conical Shock in Cross Flow

35 mm movies are convenient for two reasons: (1) any selected frame can be enlarged directly to a 4" x 5" (a linear magnification of 6) negative with a fine grain; and (2) the edited 35 mm movies can be reduced to 16 mm (a linear reduction of 2) movies with a better resolution than those copied directly from the 16 mm originals.

A total of three 16 mm movies was made during this test sequence. Although they have a common title of "Duoplasmatron-Electron Beam Flow Visualization in AFFDL/HTF," their contents are distinct. Each roll of film lasts approximately 5 minutes at 16 fps. The contents of each are listed in the Appendix.

E. COMPARISON OF SINE AND TRIANGLE WAVE FORMS

The ease with which electron beam photographs can be properly interpreted in terms of gas density variations depends upon the uniformity of the electron excitation within the field of view. A very simple sweeping system can be devised with an ac line frequency (60 Hz) sine wave applied to the sweep coil through an adjustable transformer. However, the resulting excitation is nonuniform since the sweep speed of the beam varies through the flow field. A triangular wave form which yields nearly equal sweep speeds at all locations is more suitable for electron beam flow visualization.

A waveform which is nearly triangular can be produced with the arrangement shown in Figure 22. The signal from a low voltage signal generator is amplified by a "stereo" high power (60 watt) amplifier and is capacitance-coupled to the sweep coil. The dc bias is provided by an adjustable power supply which is connected to the sweep coil through a high inductance (10 Henry) choke coil. The choke eliminates short-circuiting of the sweep signal through the relatively low impedance of the dc power supply.

Electron beam photographs of the flow about a pitot pressure probe in a resistance heated wind tunnel at The Ohio State University with both triangular and sine wave sweeps are shown in Figure 23. The wind tunnel is a special facility assembled for study of interacting gas jets. For these tests it was operated with air at a reservoir pressure of 265 psia and a reservoir temperature of 1700°R. The nominal flow Mach number was 9. The electron beam was operated at an acceleration potential of 20 kV, a beam current near 10 ma, and a sweep frequency of 1 kHz.

The better uniformity of the field of excitation with the triangular sweep is evident in Figure 23. The difference in the width of the areas excited by the beam results from the higher reactive impedance of the circuit with the triangular waveform.

IV. DISCUSSION

There are a number of reports on electron beam density measurements by photographic methods,[12,13,14] photomultiplier techniques[15] or both.[16] In general, the tunnel operating conditions, test gas, and the type of electron beam generator are different from those reported here. Additional factors to be considered before accurate density measurements can be made with confidence are discussed below.

A. FUNCTIONAL RELATION BETWEEN INDUCED INTENSITY OF RADIATION AND DENSITY

To establish the density ranges where both quantitative and qualitative density measurements are possible, the overall excitation-emission process resulting in the observed radiation must be examined in detail. This is obviously important for quantitative density determinations but is also required for flow visualization since the manner in which the intensity of the fluorescence varies with density must be known to properly interpret flow visualization photographs. Conventional optical techniques respond to the density, the density gradient or the derivative of density gradient regardless of the density level. However, the response of electron beam induced intensity depends upon the density range investigated.

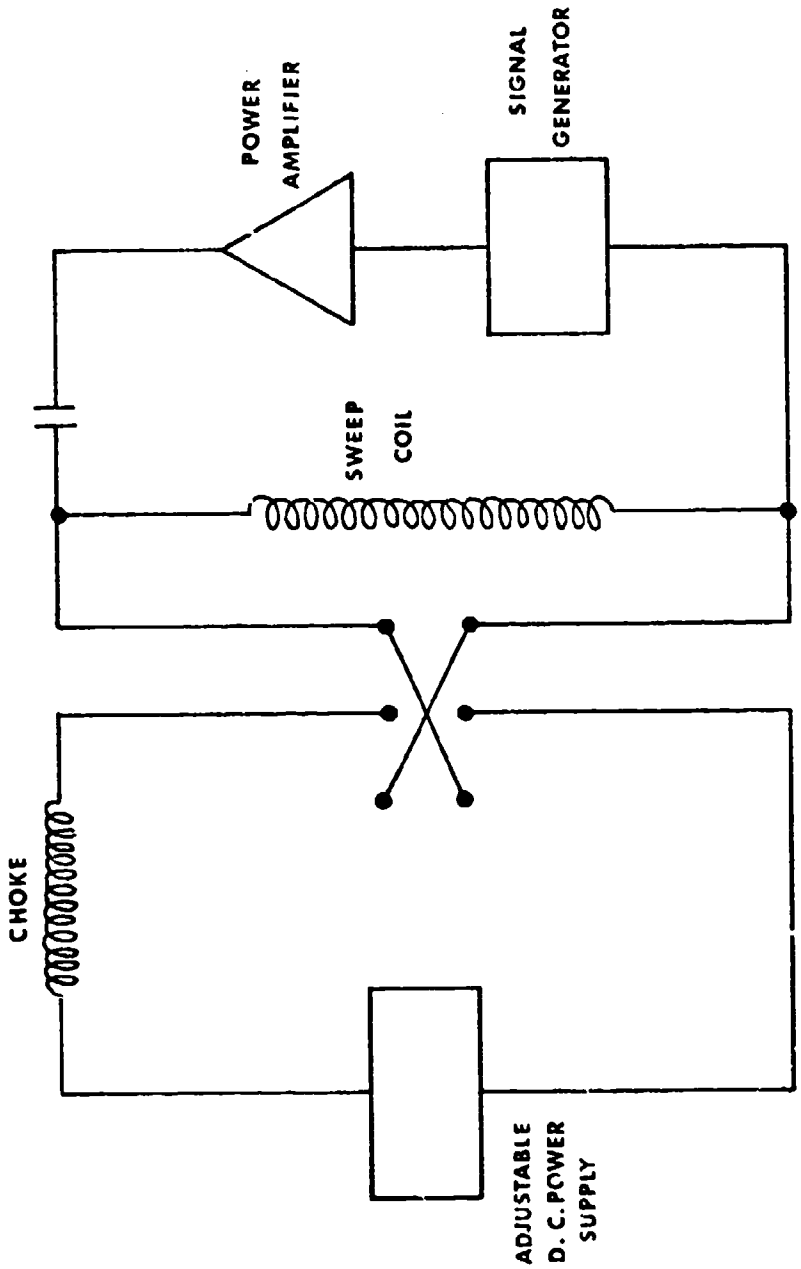

Figure 22. Sweep Circuit for Electron Beam Flow Visualization

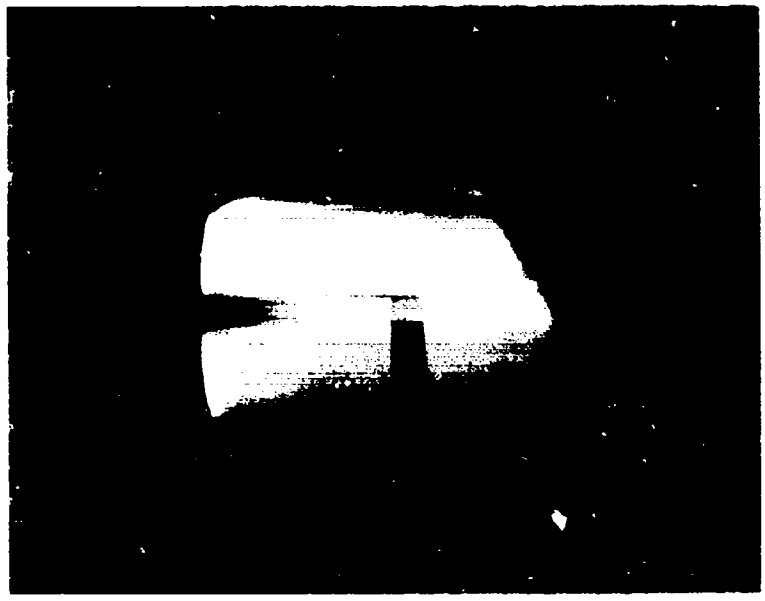

(a) Triangular Wave Form

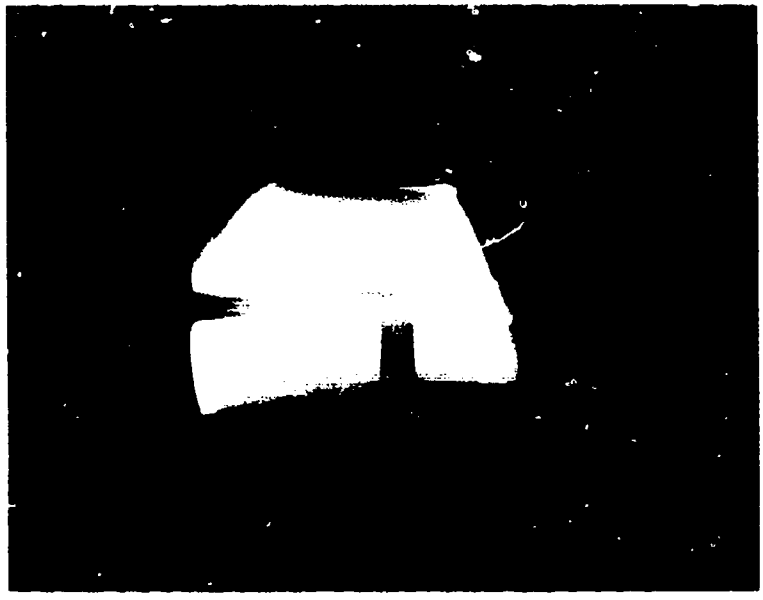

(b) Sine Wave Form

Figure 25. Comparison of Sine and Triangular Wave Forms

Of the many processes which can occur, excitation by secondary electrons and collision quenching will be considered here. For excitation of molecular nitrogen these are the only mechanisms of importance. The overall intensity of radiation induced by electron excitation can be given by[11]

$$I = \frac{c\,\rho\,J\,Q_o X_i}{1+\sum_i(\rho_i/\rho_i')} + \frac{c\,\rho^2 J\,Q_s X_i}{1+\sum_i(\rho_i/\rho_i')} \cdot \frac{\sum_i Q_{i_T} X_i}{\rho \sum_i X_i Q_{i_s} + \lambda_s^2} \qquad (1)$$

where ρ is the gas density, J is the beam current, Q_o is the cross section for excitation by primary electrons, Q_s is the cross section for excitation by secondary electrons, ρ_i' is the quenching density of species i, Q_{i_s} is the cross section for excitation of species i by secondary electrons, Q_{i_T} denotes the total ionization cross section for species i, X_i is the number density fraction of species i, λ_s is related to the mean free path for secondary electrons, and c is a constant depending on geometrical factors.

The radiation intensity due to excitation by primary electrons is contained in the first term of Eq (1), while the radiation intensity resulting from excitation by secondary electrons is given by the second term. The influence of collision quenching is contained in the term $1 + (\rho/\rho')$. If the influence of secondary electrons can be neglected, Eq (1) can be given by

$$\frac{I_o}{I} = 1 + (\rho/\rho') \qquad (2)$$

where I_o is the intensity in the absence of quenching. The quenching density ρ' is the density at which the intensity is reduced to one-half the value obtained with no quenching.

When the radiation is due almost entirely to excitation by secondary electrons, the first term of Eq (1) can be neglected giving an intensity (in the absence of collision quenching) as

$$I = c\,J\,\rho\,Q_T\,\frac{\rho}{\rho+k} \qquad (3)$$

In this equation, the term $\rho/(\rho + k)$ is the fraction of the total radiation observed where $k = \lambda_s^2/Q_s$. At very low gas densities, the range of the secondary electrons is large such that $k \gg \rho$. In this case the radiation intensity is proportional to ρ^2. At higher densities,

the range of the secondary electrons is reduced such that $\rho \gg k$ and the intensity varies linearly with density.

At gas densities less than those corresponding to 0.5 Torr at room temperature, the radiation in air is dominated by the N_2^+ first negative system in the wavelength region near 4,000 Å. In this case, excitation by primary electrons dominates and the second term of Eq (1) can be neglected. Since the self-quenching equivalent pressure* for the N_2^+ first negative system is approximately 1.2 Torr (Ref. 17), in this density region the intensity varies linearly with gas density. At equivalent pressures much over 3 Torr, the N_2^+ first negative system is quenched and the N_2 second positive system becomes most intense.

The excitation cross section for the N_2 second positive system is approximately two orders of magnitude greater for secondary electrons than it is for primary electrons. Hence, the radiation in this system is due almost entirely to excitation by secondary electrons and the radiation intensity is described by Eq (3). At very low gas densities, the intensity of the second positive system thus varies with the square of the density while at higher densities, the intensity varies linearly with the density.

The appearance of several radiation systems accompanying electron excitation obviously complicates flow visualization and quantitative determination of gas density with photographic techniques. At low gas pressures, the N_2^+ first negative system is most useful since its radiation intensity varies linearly with density. At equivalent pressures over approximately 3 Torr, the N_2 second positive system is most useful. However, in intermediate regimes, both radiation systems will contribute to the total intensity and the variation of the intensity with gas pressure will be nonlinear. Radiation from these two systems can be separated with narrow band-pass interference filters set to pass radiation corresponding to a given vibration-rotation band in the desired emission system. However, this is accomplished only at the expense of overall intensity.

B. EFFECTS OF SECONDARY ELECTRONS

When the primary electrons of the electron beam impinge upon the surface of a model, a certain fraction of the primary electrons is reflected, whereas the remainder penetrates into the solid and may cause secondary electron emission, which occurs as a result of ionization of atoms in the model material. This phenomenon occurs with both metals and non-metals.

As discussed in Ref. 14, the effects of secondary electrons must be accounted for when interpreting the additional fluorescence which typically occurs near a model surface.

---

*Equivalent pressure is defined as the pressure corresponding to the actual density and a temperature of 300°K.

V. CONCLUSION

A sweeping electron beam fluorescence technique has been successfully applied for the first time to the visualization of hypersonic airflows. The high beam currents delivered by the electron beam generator used in these studies are required for utilization of conventional photographic techniques. With this system, time resolved visualization data (i.e., high speed movies) can be obtained to allow the examination of transient flow phenomena. The ability to examine an arbitrary plane within the flow field coupled with the capability of obtaining quantitative density measurements makes the electron beam much more versatile than conventional optical techniques for the study of complex aerodynamic configurations. In fact, high quality visualization can be obtained at density levels where double-pass schlieren techniques fail to show even the bow shock wave.

Care must be used in applying the fluorescence technique to obtaining quantitative density values with photographic and/or photomultiplier methods. Spectral isolation of the radiation probably will be required to obtain accurate data. The specific vibration-rotation band employed will be a function of the gas density level. At low densities, a band from the N_2^+ first negative system should be used, while at high densities, a band from the N_2 second positive system must be employed. The effect of secondary electrons near the model surface must also be considered.

The disadvantage of the electron beam method is that it requires two photographs and a combined pitch and roll of the model to record both the compression and expansion sides of the model. This could be eliminated with a dual electron beam system at the expense of added complexity.

Besides being an improvement over conventional optical techniques in the low density range, the fact that the entire excited flow field may be easily observed with the naked eye is quite convenient. Further, flow fields can be examined directly and photographed from any angle. Control of the sweep direction allows the fluorescence technique to examine arbitrary cross-sectional slices of the flow field.

APPENDIX

CONTENTS OF THREE FLOW VISUALIZATION MOVIES

1. Color Movies (Ektachrome EF, ASA 160, 16 mm to 16 mm reproduction):

Common Parameters

Tunnel	Model
T_o = 2,500°R	9° Half-Angle Cone
M = 10	Plume Nozzle: Sonic
Medium: Air	Exhaust Plume: Air

* * *

Tunnel	Model
P_o = 100 psia	P_c = 0
R_e = 10^5/ft	α = 0

* * *

Movie

* * *

Tunnel	Model
P_o = 300 psia	P_c = 75 psia
R_e = 3 x 10^5/ft	α = 0

* * *

Movie

* * *

Tunnel	Model
P_o = 200 psia	ASSET
R_e = 2 x 10^5/ft	α = 35°

* * *

Movie

* * *

Tunnel	Model
P_o = 200 psia	ASSET
R_e = 2 x 10^5/ft	α = -35°

* * *

Movie

* * *

THE END

2. Color Movies (Ektachrome EF, ASA 160, 35 mm to 16 mm reproduction):

Common Parameters

Tunnel

T_o = 2,500°R

M = 10

Medium: Air

* * *

Tunnel	Model
P_o = 300 psia	9° Half-Angle Cone
P_∞ = .38 mm Hg	Plume Nozzle: Sonic
R_e = 3 x 10^5/ft	Plume Medium: Air
	P_c = 75 psia

* * *

Movie

* * *

Tunnel	Model
P_o = 400 psia	Ramjet Fighter
P_∞ = .49 mm Hg	α = 0° to 25°
R_e = 4 x 10^5/ft	β = 0°

* * *

Movie

* * *

Tunnel	Model
P_o = 200 psia	Ramjet Fighter
P_∞ = .24 mm Hg	α = 25°
R_e = 2 x 10^5/ft	β = 0° to 360°

* * *

Movie

* * *

Tunnel	Model
P_o = 400 psia	Ramjet Fighter
P_∞ = .49 mm Hg	α = -15°
R_e = 4 x 10^5/ft	β = 0° to 360°

* * *

Movie

* * *

THE END

3. Black and White Movies (Eastman Double-X, ASA 200, 35 mm to 16 mm reproduction):

Common Parameters

Tunnel	Model
T_o = 2,500°R	Ramjet Fighter
M = 10	
Medium: Air	

* * *

Tunnel	Model
P_o = 200 psia	α = 0° to 30°
P_∞ = .24 mm Hg	β = 0°
R_e = 2 x 10^5/ft	

* * *

Movie

* * *

Tunnel	Model
P_o = 400 psia	α = 5°
P_∞ = .49 mm Hg	β = 0° to 360°
R_e = 4 x 10^5/ft	

* * *

Movie

* * *

Tunnel	Model
P_o = 600 psia	α = -15°
P_∞ = .70 mm Hg	β = 0° to 360°
R_e = 6 x 10^5/ft	

* * *

Movie

* * *

THE END

REFERENCES

1. Rothe, D. E., "Flow Visualization Using a Traversing Electron Beam," AIAA Journal, Vol. 3, No. 10, Oct. 1965, pp. 1945-1946.

2. Sebacher, D. I., "Primary and Afterglow Emission from Low Temperature Gaseous Nitrogen Excited by Fast Electrons," Journal of Chemical Physics, Vol. 44, No. 11, June 1966, pp. 4131-4136.

3. Sebacher, D. I., "Flow Visualization Using an Electron Beam Afterglow in N_2 and Air," AIAA Journal, Vol. 4, No. 10, Oct. 1966, pp. 1858-1859.

4. Weinstein, L. M., Wagner, R. D., and Ocheltree, S. L., "Electron Beam Flow Visualization in Hypersonic Helium Flow," AIAA Journal, Vol. 6, No. 8, Aug. 1968, pp. 1623-1625.

5. Weinstein, L. M., Wagner, R. D., Henderson, A., and Ocheltree, S. L., "Electron Beam Flow Visualization in Hypersonic Helium Flow," International Congress on Instrumentation in Aerospace Simulation Facilities, ICIASF '69 Record, May 1969, pp. 72-77.

6. Muntz, E. P., "The Electron Beam Fluorescence Technique," AGARDograph 132, Dec. 1968, Neuilly-Sur-Seine, France.

7. Maguire, B. L., Muntz, E. P., and Mallin, J. R., "Visualization Technique for Low Density Flow Fields," IEEE Transactions on Aerospace and Electronic Systems, Vol. AES-3, No. 2, March 1967, pp. 321-326.

8. Lee, H. F., and Petrie, S. L., "Electron Beam Visualization in Hypersonic Air Flows," AIAA Paper No. 72-1017. Presented at the AIAA Aerodynamic Testing Conference, Palo Alto, Calif., Sept. 13-15, 1972.

9. Lee, H. F., and Petrie, S. L., "Electron Beam Visualization in Hypersonic Airflows," Journal of Aircraft, Vol. 10, No. 4, April 1973, pp. 239-243.

10. Sabick, T. F., "Automated Inspection and Data Reduction of the 5 1/2% X-24B Wind Tunnel Model," TM72-31 FXN, Nov. 1972, Air Force Flight Dynamic Lab., Wright-Patterson Air Force Base, Ohio.

11. Petrie, S. L., Boiarski, A. A., and Lazdinis, S. S., "Electron Beam Studies of the Properties of Molecular and Atomic Oxygen," AFFDL-TR-71-30, April 1971, Air Force Flight Dynamics Lab., Wright-Patterson Air Force Base, Ohio.

12. MacArthur, R. C., Stevenson, L. M., and Budell, J., "Flow Visualization and Quantitative Gas Density Measurements in Rarefied Gas Flows," ASD-TDR-62-793, December 1962, Directorate of Engineering Test, Deputy of Test and Support, Aeronautical Systems Division, Air Force Systems Command, Wright-Patterson Air Force Base, Ohio.

13. Maguire, B. L., Muntz, E. P., and Mallin, J. R., "Quantitative Visualization of Low Density Flow Fields Using the Electron Beam Excitation Technique," International Congress on Instrumentation in Aerospace Simulation Facilities, ICIASF '69 Record, May 1969, pp. 79-85.

14. Wanders, K., and Becker, M., "Influence of Electron-Beam Blunt-Body Interactions on Density Measurements in Transition Flow," Paper presented at the 8th International Rarefied Gas Dynamics Symposium, Stanford, 1972.

15. Oguchi, H., Honma, H., Bessho, J., and Ogusu, C., "Scanning-Electron-Beam Densitometer for Measurements of Density Distribution in a Rarefied Gas Flow," Report of the Space and Aeronautics Laboratory of the University of Tokyo, Vol. 2, No. 1(A), 1966, pp. 92-100.

16. Lewy, S., "Density Measurement in Aerodynamic Flows by an Electron Beam Probe," International Congress on Instrumentation in Aerospace Simulation Facilities, ICIASF '71 Record (71-C-33 AES), June 1971, pp. 125-135.

17. Rothe, D. E. and McCaa, D. J., "Emission Spectra of Molecular Gases Excited by 10 keV Electrons," CAL 165, Dec. 1968, Cornell Aeronautical Lab., Buffalo, N. Y.

TURN AROUND TIME COST STUDY SHEET

337<

☒ AD	☐ NASA*	☐ AD DEL*
☐ PB	☐ AEC*	☐ _____
☐ COM	☐ ERTS	QUANTITY PROCESSED IF MORE THAN ONE (1)
☐ JTRS*	☐ COMP. PROD.	_____

*HANDLED IN BATCHES - NOT PROCESSED THROUGH DIVISION

INPUT BRANCH

IN		OUT	
DATE	TIME	DATE	TIME
8-20-74	11:42	AUG 20 1974	2:50

DESCRIPTIVE CATALOGING BRANCH

OUT	
DATE	TIME
AUG 22 1974	1:15

INFORMATION ANALYSIS BRANCH

OUT	
DATE	TIME

PUBLICATIONS BRANCH

OUT	
DATE	TIME

PLEASE BE SURE TO POST TIME BEFORE PASSING THIS DOCUMENT ON.

THANK YOU.

MARILYN RITT